5 JET Activities

Gateable MCP based camera for VUV and soft X-ray imaging of magnetically confined plasma

M. Scholz
marek.scholz@ifpilm.pl
M. Paduch, J. Rzadkiewicz, K. Tomaszewski, and E. Zielińska

Abstract

High-resolution x-ray diagnostics for MCF devices is expected to monitor the plasma radiation emitted by W^{46+} and Ni^{26+} ions at 7.8 keV and 2.4 keV photon energies, respectively. Both, X-ray lines will be monitored by new generation energy-resolved micropattern gas detectors with 1-D position reconstruction capability. The detection structure is based on triple GEM (T-GEM) amplification structure followed by the strip readout electrode. This raport presents a design of new detectors and prototype detector tests.

Introduction

Gateable Open MCP-based device play the role of primary image detector, radiation amplifier and fast or ultra-fast shutterwhereas CCD or CMOS (High Speed Video - HSV) cameras are applied only as final image detectors, allowing the storage (in digital form) of the images of the investigated object appearing on luminescent screens of gated primary image detector

A MCP is a secondary electron multiplier consisting of an array of millions of very thin glass channels (glass pipes, typically 6 –10 μm diameters) bundled in parallel and sliced in the form of a disk [Fig.1]

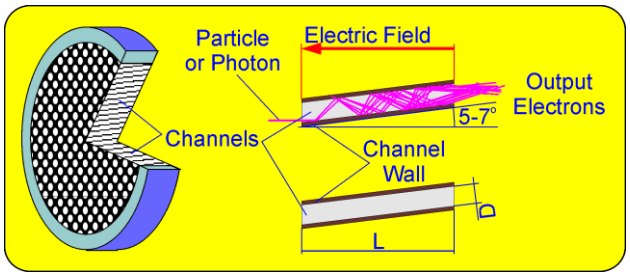

Fig.1 Scheme of multichanel plate (MCP)

Each channel works as an independent electron multiplier when a photon or particle enters a channel and hits the inner wall, secondary electrons are produced This process is repeated many times along the channel wall and as a result, a great number of electrons (multiplication factors of up to four orders of magnitude) are output from the MCP

In order to convert electron stream into light, a phosphor screen should be added. MCP and a phosphor screen must be firmly assembled inside ceramic housing, which is durably combined with a vacuum flange Such design is usually called – Open MCP-based Device In order to capture image appearing on a phosphor screen

a final image detector with appropriate optical coupling should be employed. For image registration purposes an open MCP-based device acts as a part of *"camera obscura"* layout and in consequence must cooperate with pinhole. An open MCP-based device must operate in a vacuum better than 10^{-5} mbar. In order to prevent gas leakage from experimental chamber a pinhole has to be covered by blocking foil.

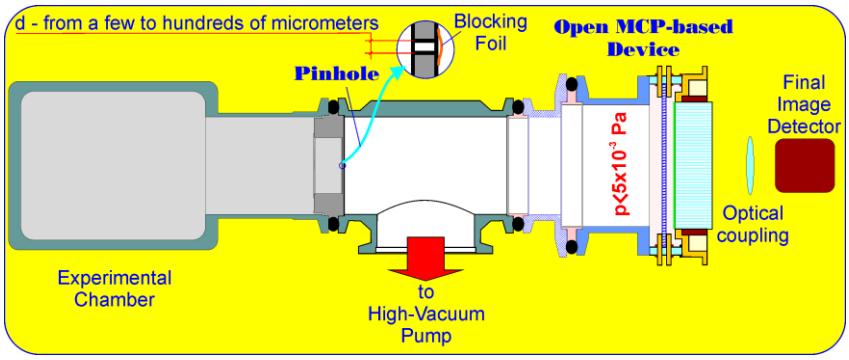

Fig.2 Scheme of soft X-ray camera with an open MPC

Soft X-ray Camera can operate as a one-frame or multi-frame camera it depends on arrangement of an open MCP-based device employed in it. In standard solution of an open MCP-based deviceboth MCP and a phosphor screen are not divided on electrically independent sectors [Fig.3].

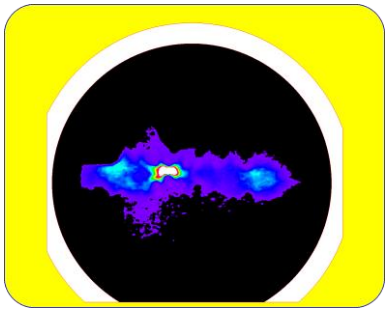

Fig.3 The image of hot plasma emitting soft X-ras recrded on a phosphor screen of MCP based camera

Sometimes, a phosphor screen is divided on electrically independent sectors. Images recording in different spectral range can be obtained for system with pinholes covered by different blocking foils [Fig.4]

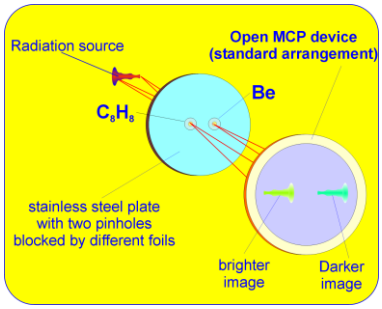

Fig.4 Scheme of the MCP-based X-ray camera with two independent sectors recording X-rays of different energies

Subtraction of both images allows to obtain final image which constitute radiation emission in low energy spectral range. The blocking foil material and its thickness modify spectral response of whole camera arrangement.

VUV-Soft X-ray Frame Camera – Final Image Detector

For final image detector, two options can be considered:

1. High resolution CCD camera;esolution of 2048x2048x10 bits or 4096x4096x10 bits; frame buffer capacity – enough to store about 512/128 frames; Frame rate – not higher than 6 fps
2. CMOS high speed video camera;esolution from 1280x1024x8 bits to 128x128x8 bits; frame buffer capacity – enough to store about 250000 frames; frame rate – not higher than 20000 fps (Table 1);

Table 1. The basic prameters of the HSC-1024 CMOS HSV Camera.

1	Sensor type	1.3 MPixels High Speed CMOS Monochrome Image Sensor			
2	Pixel size	14x14 µm			
3	Active sensor area	17.9x14.3 mm^2			
4	Spectral response	400 ÷ 1000 nm			
5	Applied image resolution	1024x1024, 512x512, 256x256 or 128x128 pixels			
6	Vertical resolution	10 bits A/D conversion; images saved as 8 bit bmp files			
7	Working parameters				
Frame Rate (frames per second)		Max. Resolution horizontal	Max. Resolution vertical	Record Time (frames)	Record Time (seconds)
540		1024	1024	4096	7.58
1930		512	512	16384	8.48
6256		256	256	65536	10.46
17485		128	128	262144	14,99
8	Shutter speed	4 µs to 25%, 50% and 100% of 1/Frame Rate			
9	On-board installed memory	4 GB			

Proposed camera will be able to record images related to the behavior of the plasma itself and plasma wall interaction, as well as its evolution caused by externally-triggered processes (e.g. heating, pellet and plasma jet injection, etc.) Such visualization (taken with high temporal and spatial resolution) will allow to:

- Find the singularities of the internal plasma structure characterized by different radiance;
- Confirm of the occurrence of events predicted by plasma modeling or simulation codes;
- Unveil phenomena that could have been “hidden” so far.

The three open MCP detectors (1D; double stack – Chevron type; equipped with 50 Ω matched anode) can be apply to MCF study. that are able to deliver analog electrical signals, linearly dependent on incoming radiation [Fig.5].

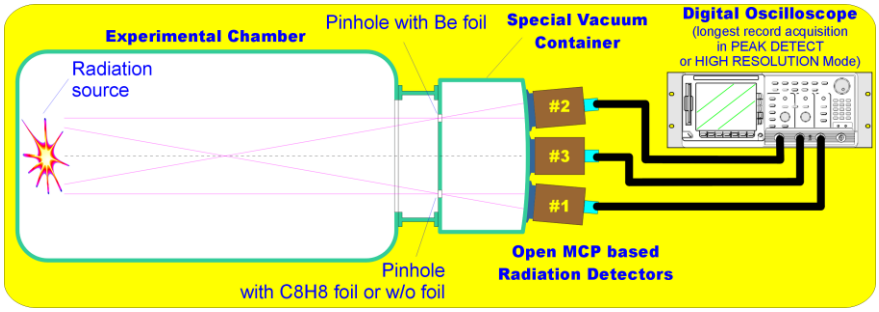

Fig.5 A complete scheme of MCP-based X-ray camera with three independent channels recording X-rays of different energies

The first detector should record radiation with possible broad spectral range; Hence, its pinhole will be blocked by a very thin, transparent foil (e.g. 1 μm polystyrene) or it should be devoid of foil (if differential pumping is practicable); The second detector pinhole will be covered by replaceable (different thickness) foils having good established low energy edge (e.g. beryllium); Such, well-known "two foils" arrangement will allow us to rough estimate in which part of the spectrum the recorded radiation is emitted; The third – "blind" detector will be used to estimate unwanted (parasite) radiation contribution (i.e. hard X-ray and neutron radiation) to recorded signals;

Conclusions

The usefulness of gateable, MCP-based devices for VUV & SXR imaging purposes has been definitely proved during dense plasma investigations

The electron density of magnetically confined plasma is usually a few orders of magnitude lower than the dense plasmas. Hence, one should expect a very strong decrease in emitted radiation level, which could prevent application of MCP-based imager from working in analog mode of operation (image recording) and simultaneously digital operation mode (photon counting & positioning) would be become much more feasible.

To solve this fundamental problem and measure VUV&SXR radiation level before final MCP-based imager development, we propose to carry out preparatory works, in which a simple arrangement being a first step toward final imaging system is proposed to be applied.

Assessment of efficiency of laser removal of fuel-inventory for mixed material samples using LIBS

P. Gąsior
pawel.gasior@ifpilm.pl
M. Kubkowska and A. Czarnecka

Abstract

The works performed in the framework of this task were concerned on the accomplishment of EFDA-JET project JW10-FT- 3.58 which in details was aimed at:

- Systematization of the results for calibrated samples with various material mix and fuel amounts,
- Verification of the possibility of application data from experiments on calibrated samples for characterization of the removal process from real-machine samples,
- Attempt to quantify LIBS indications for mixed material conditions.

In order to accomplish these aims, the experiments with laser removal of various layers of ITER relevant material mixes (C, W and Al used as Be proxy) contaminated with hydrogen and/or deuterium were

performed. As the diagnostics for the layer removal Laser Induced Breakdown Spectroscopy (LIBS) has been used. The results obtained in these experiments were compared with previous results obtained for samples from in vessel components of operating tokamaks – TEXTOR (limiter) and Asdex Upgrade (divertor).

The results shown that it is possible to detect even small amounts of deuterium/hydrogen present in the layer as well as it is possible to detect their absence when the layer is removed and the surface is reached, thus the laser removal can be assessed as effective with the use of the LIBS technique.

Introduction

Removal of fuel particles trapped in the deposits on the walls of the next-step fusion reactors is one of the crucial tasks both from safety and operational point of view. The importance of this issue is increased due to tritium radioactivity and it becomes more complicated due to mixed material conditions in the next-step fusion devices as ITER. Tokamak JET is a device which gives the most significant contribution for ITER where the problem of fuel removal has been included in its research programme.

At IPPLM the method of fuel removal by means of laser ablation and desorption has been under development. As the diagnostics for the removal process Laser Induced Breakdown Spectroscopy (LIBS) has been proposed, applied and optimized for operation in mixed-material conditions. In this purpose, experiments on numerous mixed material calibrated samples and samples from operating tokamaks such TEXTOR (limiter) and Asdex Upgrade (divertor) have been performed and their results have been compared.

The calibrated mix-material samples were prepared by collaborators and contained various mixes of carbon, tungsten and aluminium (considered as the analogue for beryllium) together with some amounts of hydrogen and/or deuterium.

After the laser irradiation by the means of Nd:YAG laser operating at 1064 nm with up to 0.6 J per laser pulse the sample's surfaces were analyzed with the optical profilometry to confirm that the layers have been removed.

Experimental set-up

A basic set-up for the experiments is shown in fig. 1. The sample was installed on the remotely controlled motion stage in the vacuum chamber out-pumped to the pressure of about 5×10^{-5} Torr. As the irradiation source a Nd:YAG laser system was applied which delivered 3.5 ns pulses of up to 600 mJ at 1064 nm. The laser beam was focused by a quartz lens of 80 cm focal length in order to obtain fluence in range up to 30 J/cm^2 (up to ~10 GW/cm^2 of power density). The light emitted by the laser induced plasma plum in front of the target was collected by the optical collimator system and transmitted via the quartz fiber to the Mechelle 5000 spectrometer equipped with Andor iStar iCCD camera. The spectral resolution ($\lambda/\Delta\lambda$) of this device was 4000 (4 pixels FWHM) with wavelength accuracy less than $\pm$0.05 nm. The area of observation of laser-induced plasma was a circle of diameter of 5 mm distanced about 3 mm from the target. The measured spectral signals were recorded and processed.

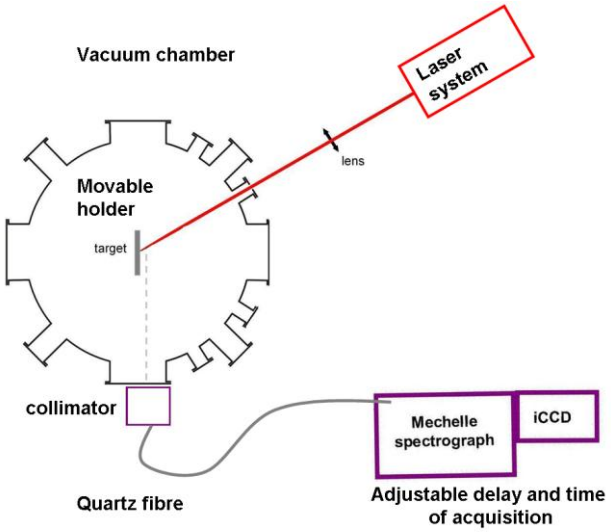

Fig. 1. Basic set-up for LIBS investigation of the laser fuel removal

The acquisition system was triggered by the standard TTL signal from the laser system. The delay time (time between the laser shot and starting the acquisition) was adjusted based on the features of the investigated samples and aims of the observation. The triggering of the system was tested by the means of the signal recorded by the ion collector which featured so called "photo-peak" resulted from the photoionisation occurring precisely in the moment of the laser irradiation.

Results

In the first step the systematization of the results for calibrated samples with various material mix and the overview of the results obtained for samples from TEXTOR and AUG have been done. It has been found, that the contribution of the deuterium/hydrogen line and its behaviour was different for this two types of samples but also stable for each of both kinds. In the TEXTOR limiter sample which contained a thick and flaking layers, the line of the hydrogen was dominating over the spectra during a few first laser shots and it was remaining on a relatively high level over 30-40 laser shots after which the layer was completely removed manifested by disappearance of the hydrogen/deuterium line. It also showed that the LIBS signal was a good indicator of the removal of the layer. This behaviour of the line was characteristic for thick co-deposits which was rather irrelevant for calibrated samples with a thin deposited layers.

More relevant to the calibrated samples was the behaviour of a LIBS signal obtained for AUG samples with a very thin co-deposit layer containing small amounts of deuterium. Two general types of AUG samples were investigated: with 4 and 200 µm of tungsten coatings on graphite substrates produced by PVD (samples 04/1, a/1, i1) and VPS (sample 01b/1), respectively. The samples constituted parts mounted in the strike-point region of the AUG divertor. Most of the laser-treated surface was localized in regions where, codeposition/implantation of fuel ions was expected during AUG operation.

For all samples, the magnitude of the deuterium line recorded in the first laser shot was at the level of the highest tungsten line (WI 429.49 nm) with ±30% variation. In contrast to the high stability of the Dα line, the lines of tungsten have not shown good repeatability but in each spectrum there were a few lines of high magnitude. This problem may be attributed to the complexity of the spectrum, which consists of many lines, close to each other located. On the other hand, the increase of delay of the recording, the contribution of lines corresponding to W^0 increased in comparison to W^{+1} lines. This behaviour is consistent with intuition, the lower propagation velocity of particles with lower charge to mass ratio.

An example of registered spectrum for this type of sample is shown in fig. 2.

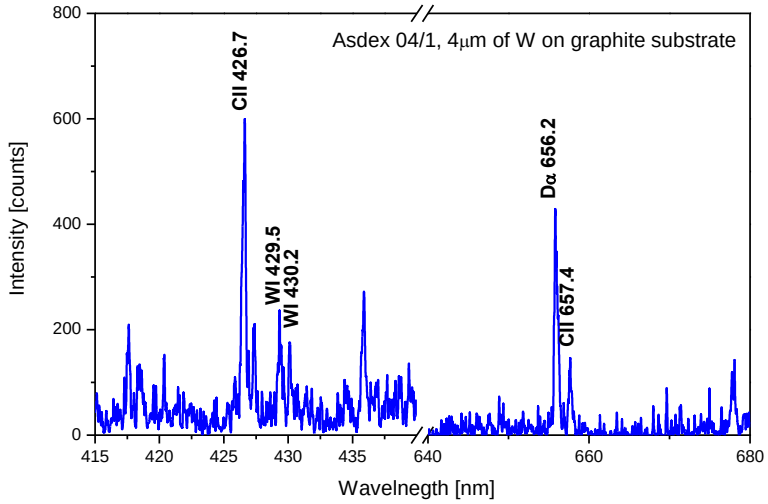

Fig. 2. Exemplary spectrum for AUG divertor sample

Similar experimental procedure was applied to the calibrated samples with various W:Al:C mixed layers contaminated with hydrogen/deuterium. The ratio of individual componentsfor investigated samples is listed in Table 1.

Table 1. Specification of samples with mixed material layers

Id	I	II	III	IV	V	VI	VII	VIII	IX
C:W:Al	1:1:1	2:1:3	3:1:2	3:1:0	1:1:0	1:3:0	1:1:1	2:1:3	3:1:2

In analysed samples the amounts of hydrogen/deuterium (the separation of the lines of the isotopes was impossible due to the resolution of used spectrometer) deduced from the line intensities were similar as those in the co-deposits on the AUG divertor, however, their removal took 3 to 5 laser shots. A curve which illustrates the decay of the hydrogen isotopes line is shown in fig.3.

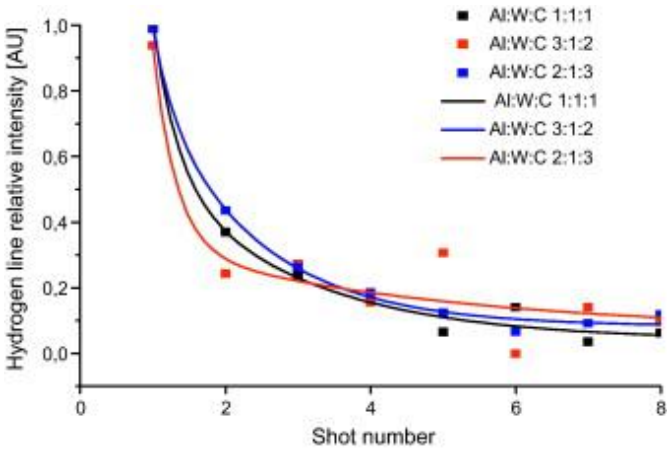

Fig. 3. Decay of the hydrogen line in various mixed material samples

The decrease in the lines that subsequent magnitudes are represented as dots in fig.3 was identified as the exponential decay. The magnitudes of the hydrogen/deuterium lines differed very insignificantly in dependence on the material mix. Slightly higher lines were observed in samples which contained the largest amount of carbon in the mix (C:W:Al = 3:1:2) which is consistent with the thesis that carbon facilitates hydrogen isotopes retention. Based on the whole research detection limits for hydrogen isotopes detection has been estimated as 10^{16} per cm^2. The amounts measured on the surface of AUG samples and calibrated samples appeared to be comparable and estimated in range of 10^{18} per cm^2. More detailed calibration was impossible due to impossibility of taking measurements for samples with well calibrated and known deuterium/hydrogen contents in a broader range.

Conclusions

The experiments allowed to confirm that the LIBS technique can be used for monitoring of the laser fuel-removal process from in vessel tokamak components. The detection limit which was estimated in the framework of the task assures that when the deuterium/hydrogen signal drops to immeasurable level, the whole co-deposited layer is removed and the surface of the component is reached.The quantification of the results is still a big challenge, but the main problems are connected with difficulties of getting calibrated samples with a broad range of deuterium/hydrogen contents for the experiments.

Collaboration

Association EURATOM – IPP Garching
Association EURATOM – FZJ Juelich

Assessment of the suitability of neutron and gamma detectors in the future experiment at JET for the validation of shutdown dose rate prediction

S. Jednoróg
slawomir.jednorog@ifpilm.pl
*A. Szydłowski**
**National Centre for Nuclear Research, Otwock*

Abstract

Estimation of the lower limit of detection of neutron and gamma detectors have been performed with the use of two gamma spectral systems: scintillation probe and germanium spectrometer. The investigated radionuclides were activated with an Am-Be neutron source. After sample activation inside the Am-Be neutron source and cooling time the sample has been measured with both systems. Relative minimum of detectable activity for scintillation counter is higher then respective values for germanium detector due to the better efficiency of the scintillation probe. The lower limits of detection for all investigated radionuclides were estimated on the basis of measured characteristics of gamma radiation.

Introduction

LLD can be understood as the lowest signal reliably exceeds N time the background standard deviation. N is typically chosen 3-5. Assuming Poison distribution, the standard deviation is equal to square root of

the collected counts. Then for background of known CPM (counts per minute), or Bq(CPM) the LLD(counts) can be expressed as follows:

$$LLD(counts) = N\sqrt{t \cdot Bg(CPM)}$$

where; t=counting time in min.

This same time the LLD(CPM) can be expressed as follows:

$$LLD(CPM) = N\frac{\sqrt{Bg(CPM)}}{t}$$

This can be converted to the lowest detectable DPM (disintegration per minutes) by dividing by AFEPE (Absolute Full Energy Peak Efficiency):

$$LLD(DPM) = \frac{N}{AFEPE(E_i)} \cdot \frac{\sqrt{Bg(CPM)}}{t}$$

This value is expressed in [Bq per sample]. The LLD depends on measurement time as well as on measurement geometry. When time of measurement increases, the value of LLD decrees respectively. It is due to better statistic of the measurement. That situation is preferred because the limit of the detection in that case is low. As was told previously the LLD depends also on registration efficiency. The efficiency degradation affects the detection limit increase because the LLD is inversely proportional to the AFEPE). This same detection sensitivity stays to be worse

Relative Minimum Detectable Activity

It has been shown (1) that the background changes with changes detector. To determine the effect of this increase in background on low-background counting, the relative figure of merit and the related value, relative Minimum Detectable Activity can be used. Both of they are related to the efficiency and to the background (or null sample) spectrum. The MDAr is proportional to the square root of the background area divided by the efficiency at the specified energy, as shown near.

$$MDA_r = \frac{\sqrt{FWMH(E_i)Bg(E_i)}}{eff(E_i)}$$

Where:

FWHM(E_i) Resolution at energy E_i

Bg(E_i) Total background at energy E_i

eff(E_i) AFEPE at energy E_i

Measurements

The two gamma spectrometry systems were used for assessment of the detection limits. The main system has been equipped with BrilLanCe380 scintillation probe and Tukan 8k MCA. The HPGe spectrometry system with I2k MCA was used for cross calibration of the previous system as well as for parallel measurements. The 51 mm diameter and 3 mm thick inconel cylindrical sample has been activated with an Am-Be neutron source of strength equal to1.5 10^7 n/s. Due to the differences in half life times of the activated radionuclides a special time sequence of the measurements has been implemented. After a few hours (2-100 h) of the inconel sample activation inside the Am-Be neutron source and tree different cooling time (1 hour, 5 days and 3 weeks) the sample has been measured with both systems. The activity of the particular nuclide was determined by the HPGe system and after that

the BrilLanCe380 was cross calibrated. This allows estimating the AFEPE (absolute full energy efficiency) for the BrilLanCe380 probe.

For all detected radionuckides the total peak area, net peak are, detection resolution, detection efficiency, activity, MDAr as well as LLD were read out from the system report files. In case of undetected radionuclides and HPGe system the MDA report was generated also.

Results

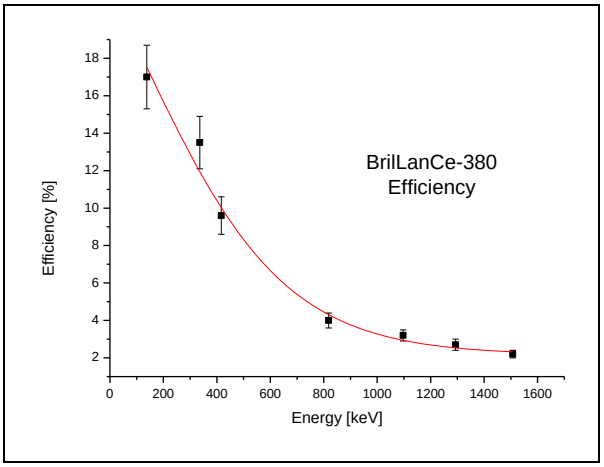

Fig. 1. The efficiency of the BrilLanCe-380 probe for the inconel sample placed on the detector end-cap

Table 1. The activity of particular radionuclides obtained as the results of 2 hour activation of inconel sample inside the Am-Be neutron source.

Nuclide Name	Id Confidence	Energy (keV)	Yield (%)	Activity (Bq /Unit)	Activity Uncertainty
CR-51	1	320.08*	9.83	5.78E+01	2.20E+00
MN-54	0.996	834.83*	99.97	1.67E+00	5.43E-02
Co-58	0.996	511.00*	29.8	7.09E+00	2.63E-01
		810.76*	99.45	7.84E+00	2.34E-01
FE-59	0.869	142.65	1.03		
		192.34	3.11		
		1099.22*	56.5	8.74E-01	4.13E-02
		1291.56*	43.2	9.00E-01	4.97E-02
CO-60	0.995	1173.22*	100	3.24E-01	1.69E-02
		1332.49*	100	3.63E-01	1.81E-02

Table 2. Spectrometric data of the inconel sample measured with HPGe system used for future calculation of MDAr and LLD respectively

Radionuclide	Energy	FWHM	Total	Net	Bground	Efficiency
	[keV]	[keV]	Area	Area		
Cr-51	320	1.24	30228	27482	2746	6.62E-02
Co-58	511	1.36	11709	8721	2988	4.47E-02
Co-58	810	1.52	19744	19193	551	3.08E-02
Mn-54	834	1.53	4793	4187	606	3.02E-02
Fe-59	1099	1.65	1272	910	362	2.44E-02
Co-60	1173	1.68	960	634	326	2.32E-02
Fe-59	1291	1.72	890	680	210	2.15E-02
Co-60	1332	1.74	846	632	214	2.10E-02

Table 3. Spectrometric data of the inconel sample measured with the BrilLanCe-380 probe. The differences in detection results between both spectrometric systems are due to the differences in sample cooling time

Radionuclide	Energy	FWHM	Total	Net	Bground	Efficiency
	[keV]	[keV]	Area	Area		
Cr-51	319.41	11.51	26464	952	25512	1.22E-01
Co-58	512.17	16.41	29240	6384	22856	8.60E-02
Mn-56	847.77	20.61	118535	104576	13959	4.70E-02
Fe-59	1097.21	24.05	6702	94	6608	3.20E-02
Fe-59	1293.93	33.12	6268	1095	5173	2.40E-02
Mn-56	1810.39	28.2	16093	11421	4672	1.60E-02

Table 4. The results of MDAr and LLD assessment for both type of the detectors. These data are also presented in Figure 2 and Figure 3 respectively

		HPGe		BrilLanCe	
	Energy	MDAr	LLD	MDAr	LLD
	[keV]		[Bq/sample]		[Bq/sample]
Cr-51	320	8.80E+02	5.39E-01	4.44E+03	1.05E-02
Co-58	511	1.43E+03	3.50E+00	7.12E+03	1.57E-02
Co-58	810	9.39E+02	4.02E-01		
Mn-54	834	1.01E+03	4.73E-01	1.14E+04	3.68E-02
Mn-56	847			11412.17	0.036759481
Fe-59	1099	1.00E+03	2.70E-01	1.25E+04	7.85E-02
Co-60	1173	1.01E+03	2.43E-01		
Fe-59	1291	8.84E+02	1.36E-01	1.72E+04	1.18E-01
Co-60	1332	9.18E+02	1.43E-01		
Mn-56	1810			2.27E+04	1.87E-01

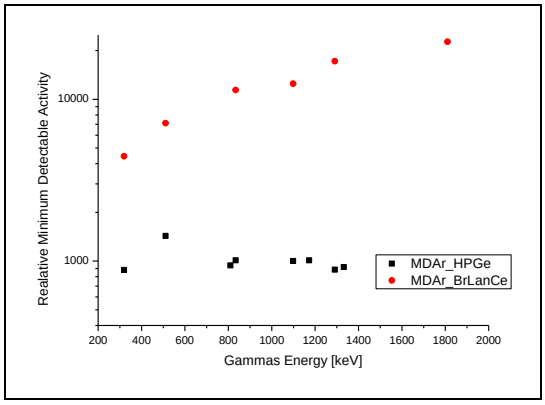

Fig.2 Relative Minimum of Detectable Activity for BrilLanCe380 is higher then respective values for HPGe detector due to the better efficiency of the scintillation probe

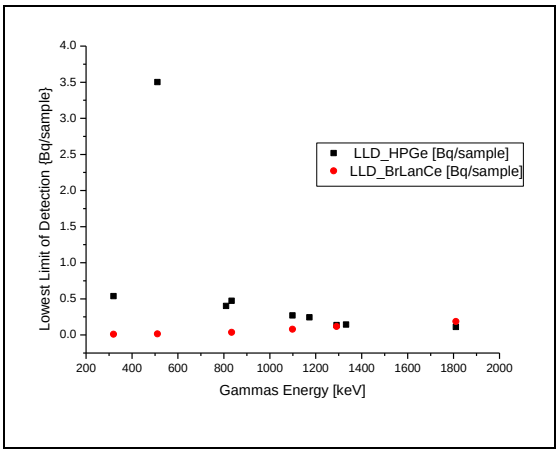

Fig. 3. Lower Limit of Detection for BrilLanCe380 probe is smaller in comparison with the HPGe. This means that the scintillate probe can reveal lower concentrations of radionuclides but some difficulty could be in identifying these radionuclides because of the lower resolution of the probe in comparison ~~to~~ with the HPGe detector resolution

Conclusion

Relative Minimum of Detectable Activity for BrilLanCe380 is higher then respective values for HPGe detector due to the higher efficiency of the scintillation probe. Lower Limit of Detection for BrilLanCe380 is smaller for scintillate probe. This means that the scintillate probe can distinguish lower concentrations of radionuclides but there will be some difficulty in identifying them because of the lower resolution of the probe in comparison to the HPGe detector resolution.

The BrilLanCe380 scintillation probe is suitable for measurement of a shut down dose provided that the level of the activity induced in the vacuum vessel walls is greater than 0.1 Bq.

The measurement of the shut down dose should be made with the probe held directly on the device wall surface because this increases the AFEPE (Absolute Full Energy Peak Efficiency) and ISAFEPE(The quantitative measure of the geometry is Integrated Square Absolute Full Energy Peak Efficiency). The measurements should be performed three times: a few hours, a few days and a few weeks after shut down respectively.

Reference

[1] S. Jednorog, M. Scholz, S. Popovichev, A. Murari, and JET EFDA contributors. Numerical Optimization of Activation Samples for the Application of the Activation Technique to Measure Neutrons in Large Fusion Devices like JET and ITER, 36th EPS Conference on Plasma Physics, Sofia, Bulgaria. (29th June 2009 - 3rd July 2009).

Gamma ray cameras: neutron attenuators

M. Scholz
marek.scholz@ifpilm.pl
R. Prokopowicz, M. Paduch, S. Jednoróg,T. Craciunescu[*], M. Curuia[**], M. Gherendi[*], and V. Zoita[*]
[*]Association EURATOM-MEdC, National Institute for Laser, Plasma and Radiation Physics, Bucharest, Romania
[**]Association EURATOM-MEdC, National Institute for Cryogenics and Isotopic Technologies, Rm. Valcea, Romania

Abstract

The JET KN3 gamma-ray cameras diagnostics system has already provided valuable information on the fast ion evolution in JET plasmas. Gamma-ray diagnostics at JET (gamma-ray spectrometry [1] and imaging [2]) have provided some of the most interesting results in experiments such as those of the TTE campaign [3].

The objectives consists in the design, construction and testing of neutrons attenuators for the vertical and horizontal cameras of the KN3 gamma-ray imaging diagnostics. This diagnostics upgrade should make possible gamma-ray imaging measurements in high power deuterium JET pulses, and eventually in deuterium-tritium discharges.

Method

Design solutions based on water neutron attenuators have been developed for the KN3 Gamma-Ray Cameras (the KN3-NA diagnostics upgrade) [4]. At the present moment all the components of the KN3-NA assembly have been manufactured and tested on a test stand which is an exact replica of the KN3 horizontal camera neutron attenuator assembly and partially replicates the installation configuration for the KN3 vertical attenuator installation configuration. Mechanical, electrical, pneumatic and hydraulic tests were performed.

The next step for the validation of the KN3-NA system consisted in radiation tests. These tests were performed by using the PF-1000 plasma-focus device at Institute of Plasma and Laser Microfusion IPPLM Warsaw and the results are reported here.

In order to measure the transfer function of attenuator, the neutron field was measured using super-heated fluid detectors, SHFFD's (also known as "bubble detectors"). SHFD are suspensions of metastable droplets which readily vaporize into bubbles when they are nucleated by radiation interactions. The active detecting medium is in the form of microscopic (20-50 μm) droplets suspended within an elastic polymer.

As the experiments provide a large amount of experimental data, it was necessary to develop o software package in order to ensure an automatic counting of the bubbles in each detector with enough precision and allowing fast data processing. The software implements a sequence of image processing techniques.

Experiments and results

The experiments were performed using the prototype version of the KN3-VC-NA (Short) attenuator. The main goal of the experiments consisted in determining the attenuation factor.

The experiments were performed taking into the assumption that the neutron source can be approximated with a point source: the source was estimated by IPPLM staff to have a cylinder shape (2

cm diameter, 5 cm length) and the direction from the point source is perpendicular to the detectors (see Fig. 5 – left).

Preliminary experiments were performed during May 2010 and were dedicated to the characterization of neutron field specific to the PF-1000 device. During extensive experiments neutron spectra were recorded, using the detectors with different energy thresholds (BDS bubble detector spectrometer).

The experimental results revealed that even without the attenuator, the energy distribution has a strong component in the low energy range (E < 0.1 MeV) (Fig. 1). It was assessed that the main reason for this component are the surrounding structures. The low-energy neutron field would have a strong influence on measurements concerning the attenuation factor.

Therefore further experiments were performed during the second half of the year 2010 in order to find an optimum experimental setup and to determine the transfer function of the attenuator. A new measuring location, placed also on the axis of neutron emission was used. The location was chosen in order to minimize the influence of the neutron scattering surrounding structures. Additionally the detectors were placed inside a paraffin collimator in order to ensure additional shielding.

In order to test this configuration neutron spectra were recorded. It worth to be mentioned that for these experiments new spectrometric detectors (BDS), with increased efficiency and energy threshold above 1 MeV were purchased and used.

The results are illustrated in Fig. 2. The spectrum was recorded in multiple shots which cumulates a total neutron production of 4.80 10^{11}.

As it can be observed the spectrum has a small component in the low energy range (E < 0.1 MeV) . This suggests that neutron scattering influence was diminished significantly and the measurement environment is appropriate for determining the attenuator transfer function.

The attenuation factor was determined by recording the detector response, with and without attenuator, in the energy range above 1 MeV. A representative result is presented in Fig. 10. The detectors were exposed to multiple shots in order to ensure a good statistic. The total neutron production was 0.81x10^{12} for the measurements without attenuator and 1.03x10^{12} for the measurements with attenuator respectively. The detector responses were scaled in respect with the neutron production characteristic during their exposure and also according to their sensitivity. The detector response function was used for detector response deconvolution. The evaluation of the attenuation factor is summarized in Table 1.

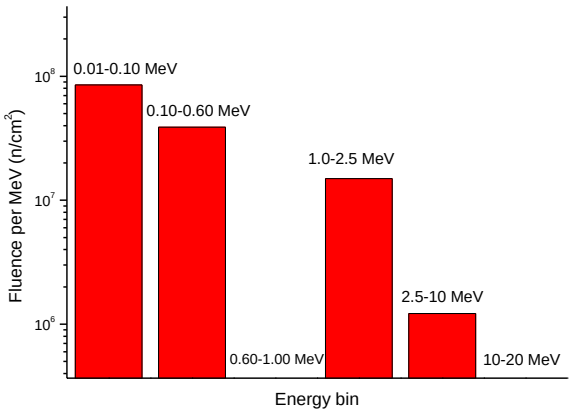

Fig. 1. Neutron spectra showing a significant component in the low energy range (E < 0.1 MeV) due to neutron scattering induced by surrounding structures

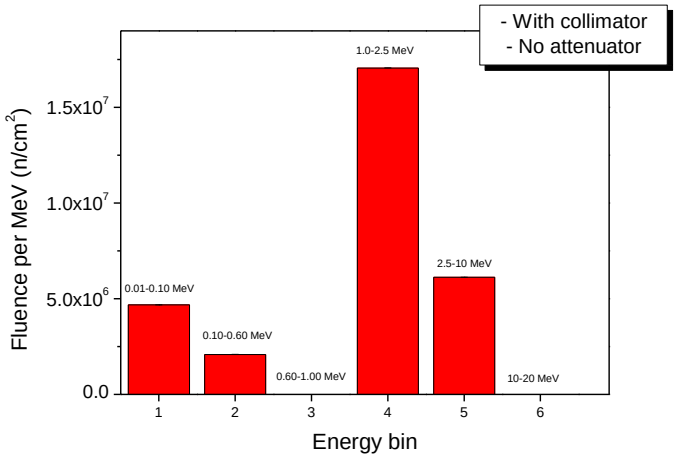

Fig. 2. Neutron spectra obtained using an experimental configuration #2

Table 1. Attenuation factor evaluation

Geometry	Total neutron production	Coorected no of bubbles	Factor
Without attenuator	$0.807\ 10^{12}$	88 ± 1.43	112 ± 31
With attenuator	$1.032\ 10^{12}$	0.79 ± 0.43	

The evaluated attenuation factor proved to be in agreement with the attenuation factors considered to be attainable within the project constraints (~ 10^2).

Collaboration

Association EURATOM-MEdC, National Institute for Laser, Plasma and Radiation Physics, Bucharest, Romania

Association EURATOM-MEdC, National Institute for Cryogenics and Isotopic Technologies, Rm. Valcea, Romania

References

[1] V.G. Kiptily , F.E. Cecil, O.N. Jarvis , M.J. Mantsinen, S.E. Sharapov, L. Bertalot, S. Conroy, L.C. Ingesson, T. Johnson, K.D. Lawson, S. Popovichev, *γ-ray diagnostics of energetic ions n JET*, Nucl. Fusion (2002) **42**, 999.

[2] O.N. Jarvis, J Adams, P.J.A. Howarth, F.B. Marcus, E. Righi, G.J. Sadler, D.F.H. Start, P. Van Belle, C.D. Warrick, N. Watkins, *Gamma ray emission profile measurements from JET ICRF-heated discharges*, Nucl. Fusion, (1996) **36**, 1513.

[3] V. G. Kiptily, Yu. F. Baranov, R. Barnsley, L. Bertalot, N. C. Hawkes, A. Murari, S. Popovichev, S. E. Sharapov, D. Stork, V. Yavorskij, *First Gamma-Ray Measurements of Fusion Alpha Particles in JET* Trace Tritium Experiments, Phys. Rev. Lett. (2004) **93**, 115001.

[4] V. Zoita, M. Anghel, T. Craciunescu, M. Curuia, T. Edlington, M. Gherendi, V. Kiptily, K. Kneupner, I. Lengar, A. Murari, A. Pantea, P. Prior, S. Soare, S. Sanders, B. Syme, I. Tiseanu. Design of the JET upgraded gamma-ray cameras. Fus. Eng. Des.(2009) **84**, 2052.

Development of soft X-ray triple GEM gas detector for energy resolved soft X-ray plasma diagnostics

J. Rzadkiewicz
jacek.rzadkiewicz@ifpilm.pl
W. Dominik[*], M. Scholz, K-D. Zastrow[**], M. Chernyshova, T. Czarski, H. Czyrkowski[*], R. Dąbrowski[*], K. Jakubowska, L. Karpiński, G. Kasprowicz[****], K. Kierzkowski[*], K. Pozniak[****], Z. Salapa[*], W. Zabolotny[****], P. Blanchard[***], and S. Tyrrell[**]
[*] Warsaw University, Faculty of Physics, Institute of Experimental Physics, Warsaw, Poland
[**] Euratom/CCFE Fusion Assoc., Culham Science Centre, Abingdon, UK
[***]Association EURATOM-Confédération Suisse, EPFL, CRPP, Lausanne, Switzerland
[****]Warsaw University of Technology, Institute of Electronic Systems, Warsaw, Poland

Abstract

An arrangement consists of open MCP-based detectors can be considered as a candidate for imaging of VUV&SXR radiation emitted by magnetically confined plasma. Analog electrical signals taken from these detectors will enable us to estimate radiation level emitted in different spectral ranges and evaluate noises level induced by hard X-ray and neutron radiation. The obtained results should be a base to answer on fundamental question: whether and what kind (analog – imaging oriented or digital – photon counting & positioning oriented) VUV & SXR imager could be applied to magnetically confined plasma study.

Introduction

High-resolution X-ray spectroscopy is a powerful tool for diagnosing the properties of tokamak plasmas. The characteristic X-ray radiation emitted by highly ionized metal impurities provides accurate information on crucial plasma parameters such as impurity concentrations, ion temperature, and the toroidal rotation velocity [1,2]. For example, the high-resolution diagnostic at JET is based on a spectrometer in the so-called Johann geometry with a very large focal length 2R=25m where R is a Rowland circle radius [3]. The ITER-oriented JET research program brings a new important requirement for the X-ray diagnostic which is expected to monitor the impurity level of tungsten – the plasma-facing material of the new JET divertor. Therefore, besides the upgrade of the Ni monitoring diagnostic, in order to implement the W impurity monitoring one has to design and construct X-ray detectors dedicated for high and low energy X-ray diagnostic channels.

The main aim of the high-resolution X-ray diagnostic is to provide monitoring of the radiation emitted by Ni^{26+} and W^{46+} at 2.4 keV and 7.8 keV from the hottest region of the tokamak plasmas. The X-ray diagnostic should also provide information on the continuous radiation. Therefore, the final design of the position sensitive X-ray detectors was driven by the following requirements: large detection area (206x92 mm^2), good space resolution, high charge gain possibility, detection stability for a wide range of photon rates and reasonable energy resolution.

Technical description of x-ray gas detectors and detection efficiency

The construction of both detectors for high-resolution x-ray diagnostics at JET is based on the Triple GEM (T-GEM) geometry (Fig. 2). The T-GEM detectors should resolve the space and energy of the X-ray photons diffracted from the cylindrically bent crystals (see Fig. 1). The T-GEM structure allows one to reach a high total gas gain (exceeding 10^4) with a very low discharge probability. Additional advantage of such structure is that only fast electronic component of avalanches in gas drifts towards strips thus, the space charge effect due to positive ions is strongly reduced. In the prototype phase of the project it was demonstrated

that the T-GEM detector filled with Ar/CO2 (13%-30%) gas mixture at atmospheric pressure provides a good charge gain. The T-GEM structure with inter-GEM spacing of 2 mm and the induction gap width of 2.5 mm should match the operational requirements of the high-resolution X-ray diagnostics. Each detector consists of 128 10cm-long-strips with strip pitch of 0.8 mm.

Preliminary detector tests led us to the design of the final detector modules. An expanded view of the T-GEM detector and the assembled final T-GEM module is presented in Figs. 2. As a construction material for detectors (frames and assembly bolts) *DELRIN* material (without metallic components) was chosen in order to avoid a secondary fluorescence. The electrical connection pins and the gas inlets are visible in Fig. 2.

Technology of the thin mylar window stretching and gluing to the dedicated frame assured good window flatness when operated under small overpressure due to the gas circulation. The detector window was additionally supported by system consisting of two ribs installed on the outer side of the window. In this way good window flatness was assured. The drift-gap frame and electrode frames have larger opening than the window frame that should reduce edge effects related to the electric field distortion in the vicinity of the dielectric surface.

The closing frame closes the detector and allows one to introduce a gas mixture through the passage on the strip plate. In the Figure 4 one can also see the AFE electronics crate mounted on the detector. Such installation assures good protection of the high voltage lines. Analogue signals from strips will be transmitted via special SMD connectors to the back-plane serving to connect individual amplifier/shaper channels. The AFE channel bandwidth is 15 MHz will be tuned to match characteristics of the primary strip pulse and the 100 Mhz sampling rate of digitization in the 10 bit ADCs. Dedicated algorithm of cluster size and cluster amplitude will be implemented in the detection unit for the precise energy reconstruction.

In order to optimize the detector efficiency the studies of the gas mixture and detector window materials have been performed. The Ar70%+$CO_2$30% mixture with maximum considered layer thickness of 1.5 cm has been chosen In order to minimize the absorption in the window the technology of the thin (12 μm and 5μm) aluminized mylar detector window with the applied HV of the order of 5kV has been verified in test X-ray measurements. The results of calculations of the detection efficiencies for Ni (with 12μm mylar window) and W (with 5μm mylar window) monitor X-ray detectors are shown in Fig. 3. The X-ray energies of the main monitoring X-ray lines are also shown.

Prototype detector tests

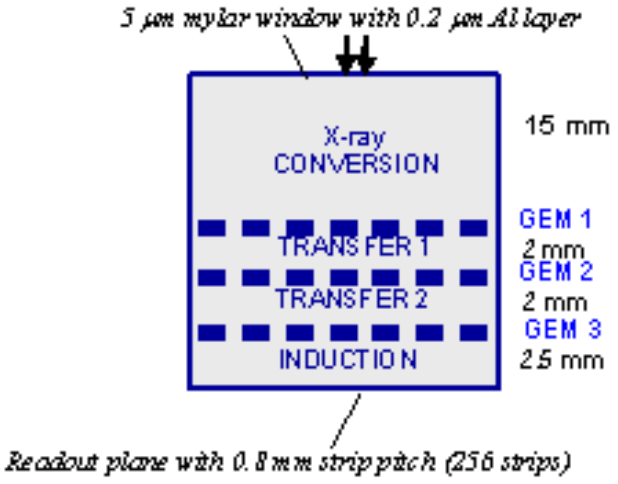

Fig. 1. Scheme of the T-GEM detector structure

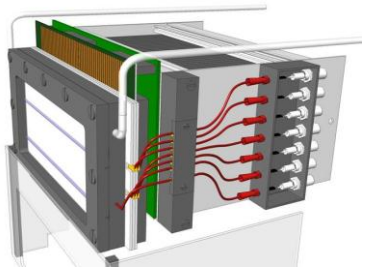

Fig. 2. View of the assembled final T-GEM module

The T-GEM x-ray prototype detector with 10x10 cm2 detection area was tested to study energy and space resolution and the Ar/CO2 (30%) gain as a function of applied voltages (GEMs, induction, drift and transfer voltages). Tests were mainly performed by means of the ^{55}Fe x-ray source and 2.5 kV X-ray generator (100uA) with X-ray photon energy peak at about 2 keV.

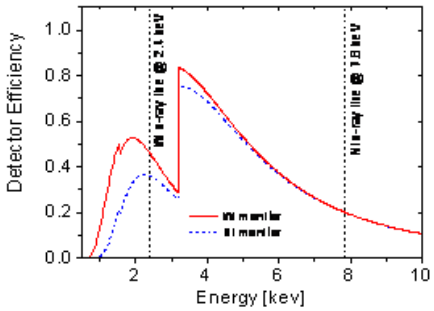

Fig.3. Calculated photon detection efficiencies as a function of photon energy for Ni and W monitor x-ray detectors with 12□m and 5□m mylar windows, respectively

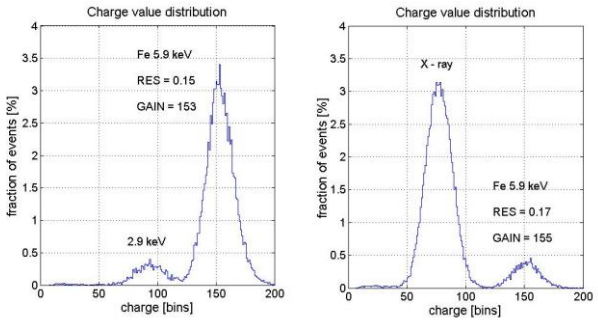

Fig. 4. Charge (energy) distribution measured for a 55Fe source (left) and for the 2.4 kV X-ray tube and 55Fe source together

Fig. 4 shows the typical height spectrum for Ar/CO2 (30%) gas mixture measured with ^{55}Fe x-ray source (left side) and X-ray generator (right side), respectively. The 5.9 keV x-ray peak is well separated from the escape peak of Ar and from the x-ray peak (at ~2 keV) generated by X-ray tube. The energy resolution of 0.15 and 0.17 were obtained for ^{55}Fe and combined ^{55}Fe with X-ray generator measurements, respectively. The space resolution was analyzed with X-ray tube source (2.5 kV, 100uA) (Fig. 5). The surface of the prototype detector window was irradiated by X-ray bundle through the collimator (diameter of 0.7 mm). Two measurements with the same voltage settings were performed (HV(1:7) = [1200, 360, 700, 360, 700, 360, 1000] [V]) and a slightly different collimator position. The measurement has shown the local detector position resolution of 0.3 stripe (0.25 mm).

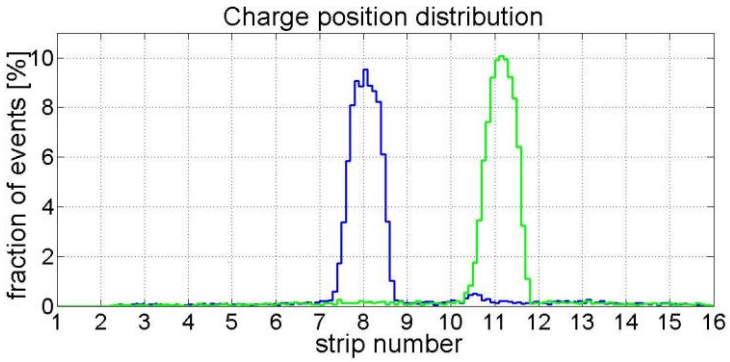

Fig. 5. Charge position distribution for selected X-ray source position. X-ray tube (2.5 kV, 100 uA) with a 0.7 mm diameter collimator was used as a radiation source

The relative gain of the prototype detector with Ar/CO2 (30%) was measured as a function of applied GEM voltages by using the ^{55}Fe x-ray source. Results of these measurements at V_{ind}=1.2 kV (see Fig. 6) indicate the monotonic dependence of the gain in the range of voltages applied.

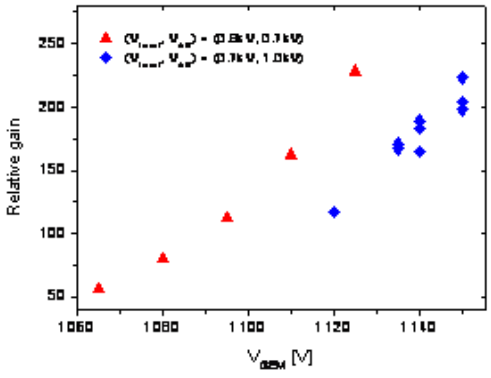

Fig. 6. The relative gain versus the total GEM voltage

The detector prototype and radiation source was also used for the electronic hardware verification and preliminary development of measurement algorithms implemented in FPGA. The FPGA available on FMC board is devoted to input signal processing and real time raw data acquisition for debugging purposes. The FPGA development board will be used in X-ray detectors for the photon energy and position estimation. In order to verify the operational stability of the detectors, a medium-term test has been performed for more than 100 hours. The charge gain and the energy resolution for the 5.9 keV line were monitored. The detection energy resolution remained stable with the long-term (few dozens of hours) improvement tendency and the relative charge gain exhibited dependence on the atmospheric pressure to temperature ratio with about 15% variability.

Conclusions

For both low- (W^{46+} at 2.4 keV) and high (Ni^{26+} at 7.8 keV) photon energy diagnostic channels two T-GEM detectors with 100x100 mm2 detection area and 128 strip channels each. Two materials are proposed as final detector windows, namely Mylar 5 μm + Al 0.2 μm (M5Al) and Mylar 12 μm + Al 0.2 μm (M12Al). The final detector windows should be supported by two slabs (0.8 mm in diameter) installed on the outer side of the window. As a working gas the ArCO2 (70:30) gas mixture with 15 mm thickness of gas-mixture layer has been chosen. The expected detector efficiencies are 45% at 2.4 keV (W monitoring channel) and 20% at 7.8 keV (Ni monitoring channel), respectively.

Collaboration

Warsaw University, Faculty of Physics, Institute of Experimental Physics, 00-681 Warsaw, Poland

Euratom/CCFE Fusion Association, Culham Science Centre, OX14 3DB, Abingdon, UK

Association EURATOM-Confédération Suisse, Ecole Polytechnique Fédérale de Lausanne (EPFL), CRPP, CH-1015 Lausanne, Switzerland

Warsaw University of Technology, Institute of Electronic Systems, 00-665 Warsaw, Poland

References

[1] K-D Zastrow, et al., J. Appl. Phys. (1991) **70**, 6732.
[2] K. W. Hill et al., Rev. Sci. Instrum. (2008) **79**, 10E320.
[3] R. Bartiromo, et al., Rev. Sci. Instrum. (1989) **60** (2), 237.
[4] G. Kasprowicz et al., Proc. SPIE, vol. 8008, 2011, 80080J.
[5] www.creotech.pl
[6] K. Pozniak et al., Proc. SPIE, vol. 8008, 2011, 800808.
[7] K. Jakubowska et al., 35th EPS Conference on Plasma.

Development and application of neutron diagnostics based on activation method for magnetic confinement devices

S. Jednoróg and M. Scholz
slawomir.jednorog@ifpilm.pl
S. Popovichev[*], A. Murari[**] and JET EFDA contributors
[*] EURATOM/CCFE Association, Culham Science Centre, Abingdon, Oxon, UK
[**] Consorzio RFX-Associazione EURATOM ENEA per la Fusione, I-35127 Padova, Italy

Abstract

The activation technique is widely used in large magnetic confinement devices for the measurement of the neutron yield and the evaluation of the neutron spectra for DD and DT operations. On JET the activation technique is the reference measurement for the calibration of the other neutron diagnostics.

In the case of a spectrometric system for the activation technique, the gamma ray detector together with the particular sample characterized by its shape, elemental composition and its position relative to the detector must be calibrated each time if even one part of the above setup is varied. The efficiency calibration is unique function for the couple consists of particular detector and particular sample hold in particular position regarding to the detector.

Today High Purity Germanium detectors with high efficiency and resolution are available. Those detectors can be numerically characterized which allows estimation of energy-efficiency calibration for practically an unlimited number of sample with different shape, composition and position relative to a detector.

In this paper the size optimization of cylindrical indium samples for low neutron flux measurements is described. It was prove that for above indium sample laying on the High Purity Germanium Detector endcap only the diameter of sample can be chosen by means of optimization technique.

The parameter Integrated Absolute Full Energy Peak Efficiency and Mass Integrated Absolute Full Energy Peak Efficiency have been used in this work as the useful qualitative and quantitative estimators of the sample properties. Based on these two parameters a systematic analysis samples made of aluminium, indium, yttrium, titanium, zirconium, iron, cadmium, nickel, cobalt, hafnium and gold have been performed.

The newly introduced mixed sample as the homogeny composition of desirable elements with strictly defined percentage composition has been energy-efficiency calibrated by means of numerical method. This sample it is characterized by relatively high Absolute Full Energy Peak Efficiency. The mixed sample activation technique was widely used in experiments on JET Campaign 20-25.

Introduction

In the activation technique, samples of suitable materials are placed close to the plasma and withdrawn for remote analysis. This method is widely used in large magnetic confinement devices for the measurement of the neutrons yield and evaluation of the neutron spectra for DD and DT operations [1]. The activation sample is optimized in isotopic composition, shape and size. This challenging task requires a careful evaluation of the efficiency of the gamma ray registration. In the previous experiments at JET only stacks of different discrete foils were used [2]. Nowadays available High Purity Germanium (HPGe) detectors with high efficiency and resolution can be characterized numerically very well in terms of efficiency calibration. This allows the applications of samples with a mix of different element compositions, shapes and with relatively short half live time.

The methodology presented in this paper allows the evaluation of the absolute full-energy peak efficiency (AFEPE) for a broad spectrum of samples with good accuracy. The following capabilities of the new software are presented: the analysis of the accuracy of the Laboratory Sourceless Object Calibration Software (LabSOCS); three dimensional (3D) AFEPE for ideal and realistic samples; optimization of the geometry for realistic activation samples; AFEPE for samples made from 11 different elements activated during recent JET campaigns; evaluation of AFEPE for mixed samples used on JET in comparison with aluminum and gold samples. The technique presented has been implemented on JET and has provided a supplementary source of information for the JET activation diagnostic. Particularly interesting results have been obtained in the determination of the neutron field characteristics of JET high performance discharges [3].

System for gamma ray detection and its numerical efficiency calibration

The Detection System for Gamma Ray Registration (DSGR) consists on an InSpector 2000 Multichannel Analyzer (MCA), a High Purity Germanium (HPGe) Coaxial Detector System, Genie-2000 Gamma Analysis Software, the Numerical Characteristic (NCh) of the HPGe detector, Laboratory Sourceless Object Calibration Software (LabSOCS) and the Shielding System. The Shielding System consists of the specially designed Electromagnetic Shield (EMS) and the typical shield for radiation background reduction. The HPGe detector with radiation shield, MCA, and steering computer were placed inside the EMS and supplied with power on Uninterruptible Power Supply (UPS). This protects DSGR against electromagnetic interference even propagated throughout the power network.

The design of particular sample consists of its shape, chemical, and elemental composition. It is called in this paper as the sample geometry. The position of the particular sample relatively to the detector is called measurement geometry. The elemental composition strictly influents on type of nuclear reaction caused by neutrons and after that obtained information regarding neutron spectrum reached in result both of radioactivity measurement and calculation. The considered in this paper AFEPE strongly depends both on sample geometry and measurement geometry as well.

In this paper we define an efficiency of photon registration as AFEPE that is in agreement with its definition taken from the gamma spectrometry handbook [4] and expressed as:

$$\varepsilon ff(E) = \frac{R}{A \cdot P_\gamma} \quad (1)$$

where: R - full energy peak count rate (s),

A -activity (Bq),

P_γ - probability of particular gamma ray emission.

Subsequently the numerical assessment of the registration efficiency is named IAFEPE and it is expressed as follows:

$$IAFEPE = \int_{E_{\min}}^{E_{max}} eff(E)dE \quad (2)$$

where: E_{min}, E_{max} – the range of efficiency calibration which is particularly this same as the energetic sensitivity of considered detector.

Meanwhile MIAFEPE represents capacity of sample for activation and after that it measurability by means of particular detector and it is expressed as follows:

$$MIAFEPE = \int_{E_{\min}}^{E_{max}} m \cdot eff(E)dE \quad (3)$$

where: m – sample mass (g).

The HPGe detector has been supplied with its Numerical Characteristic (NCh) which allows the determination of the sample activity without performing the efficiency calibration in situ. The NCh of the detector was provided by the manufacturer. At the factory, the exact dimensions of this particular detector, including its mounting and housing, were included into an MCNP model named LabSOCS. As stated in [5] and [6], LabSOCS energy-efficiency calibration data-points have typical accuracy of ~7% Standard Deviation (SD) for energies < 150keV, ~6% SD for 150-400keV, ~4% SD for 400-7000keV. Our energy-efficiency calibration tests, performed with a certified calibration sources placed in Marinelli geometry, are in good agreement with LabSOCS data. The comparison of both calibrations, performed using a calibration source and calculated with LabSOCS, is shown in the Fig. *1.*

Three-dimensional efficiency calibrations for ideal and realistic samples

The energy-efficiency calibration for a particular detector and sample is defined as a function of AFEPE versus the photon energy in a broad energy range. Usually the efficiency curve is a logarithmic polynomial of fifth or lower order and can be expressed as:

$$Eff(E) = \sum_{i=0}^{5} A_i \cdot \ln(E)^i \quad (4)$$

where: A_i - parameter of the fitting, E – photon energy.

The shape of this curve for constant photon energy is very dependent on the sample geometry (composition and shape) as well as measurement geometry. The three-dimensional (3D) curve of

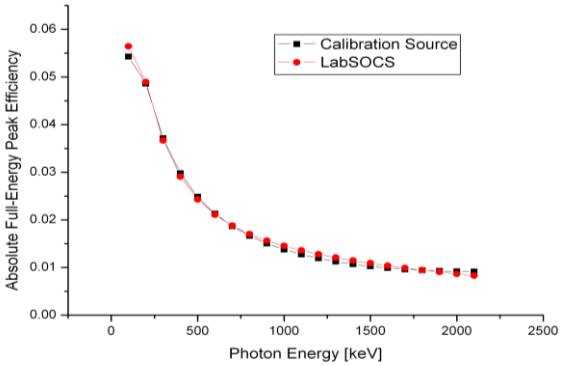

Fig. 1. Efficiency calibration obtained with a certificated source (black) and LabSOCS (red)

efficiency can be obtained by scanning the various geometrical parameters of the sample one at the time. As an example, Fig. 2 represents the 3D efficiency for an ideal point source as a function of photon energy and distance between the source and the detector endcap. The dependence of the energy efficiency versus the sample diameter of a realistic finite thickness and diameter indium sample is shown in Fig. 3. In this case, the thickness of the sample has been neglected and the sample has been positioned on the surface of the detector endcap. The difference in the shapes of the curves confirms the fact that for realistic samples the self attenuation of the photons dominates, whereas in the ideal sample case the geometrical factor represented by the simple inverse square law plays the main role.

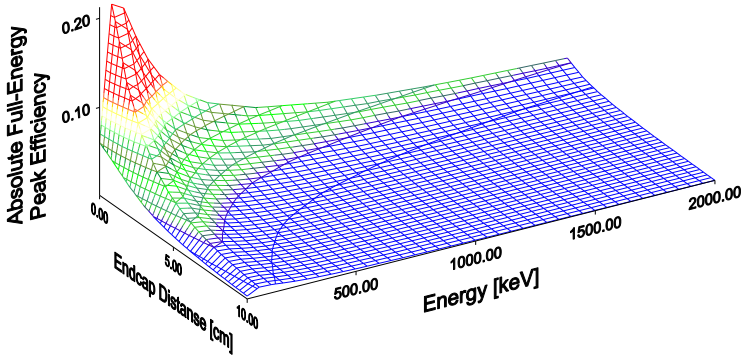

Fig. 2. Absolute full energy peak efficiency of an ideal point radiation source as a function of photon energy and sample distance from detector endcup

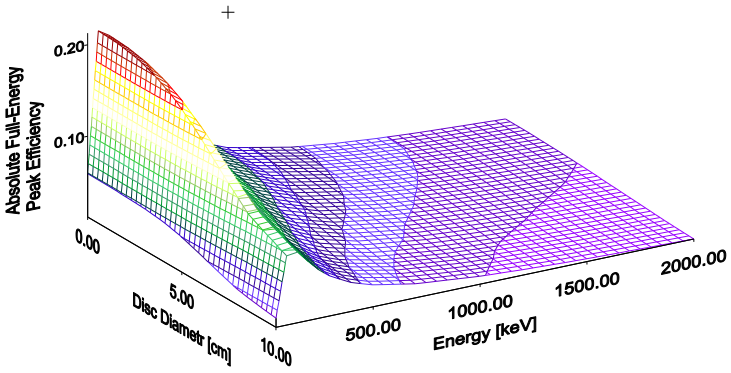

Fig. 3. Absolute full energy peak efficiency of a realistic thin indium disk as a function of photons energy and sample diameter.

Optimization of the geometry for realistic activation samples

The following nuclear reactions $In^{115}(n,\gamma)In^{116}$, $In^{113}(n,\gamma)In^{114}$, $In^{115}(n,n')In^{115m}$, $In^{113}(n,n')In^{113m}$, play an important role in the neutron interactions with indium nuclei. They are reactions of radiation capture of neutrons by In^{115} and In^{113} nuclei and neutron scattering by the indium nuclei. The inelastic scattering reactions are threshold reactions, i.e. they occur only for the neutron energy exceeding a certain energy threshold. In the case of In^{115m} the detection of photons with energy of 336 keV reveals the presence of neutrons with energies above ~400 keV whereas detection of photons with energies of 391 keV from In^{113m} indicates the presence of neutrons with energies exceeding ~800 keV.

Thus reactions induced by neutrons of certain energies translate into gamma rays of specific energies. The reliable detection and identification of the maximum number of such reactions require finding the best sample geometry (sample optimization) which will ensure both high sample activation and effective registration of photons by means of a HPGe detector.

n our case it is essential to optimize the sample diameter. This has been done by careful analysis of the dependence of AFEPE on the sample diameter for constant photon energy. The typical cross section of such an efficiency surface for an indium sample versus its diameter is presented in Fig. 4. These kinds of curves have been analyzed as described in the following. Equation 2 describes the dependence of AFEPE on realistic cylindrical indium sample diameter for constant photon energy:

$$D(x,\ E=const) = y_0 + \sqrt{\frac{\pi}{2}} \cdot \frac{A \cdot \exp\left(-\frac{2(x-x_c)^2}{w^2}\right)}{w} \qquad (5)$$

where: x- is the diameter of the sample,

x_c, A, y_0, w are the parameters of the Gaussian fit.

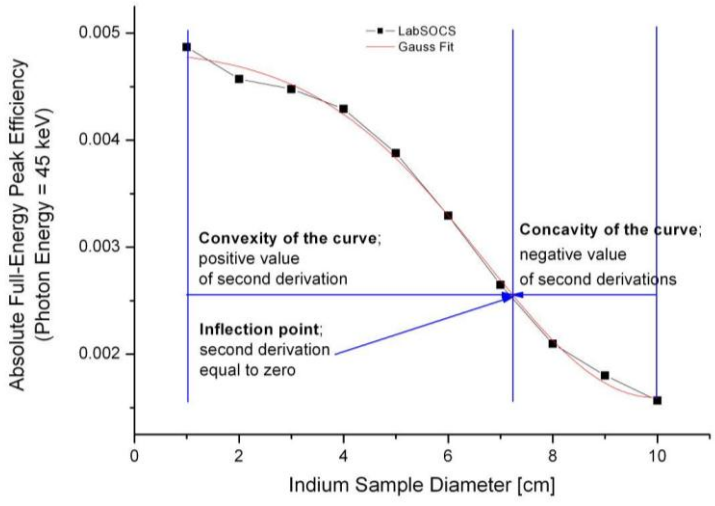

Fig. 4. Typical cross section of the efficiency surface for constant photon energy allows determining the dependence of the efficiency on the diameter for a realistic indium sample

The fitting algorithm has been particularized for the particular photon energies used previously for the efficiency energy calibration.

As shown in Fig. 4, the photon registration efficiency curve changes both its shape and character near the inflection point. Here the inflection point is defined as the point where the second derivative of the above function is equal to zero (see Fig. 4).

A series of inflection points for constant photon energy is shown in Fig. 5. It represents the range of optimal sample diameters. The value of optimal diameter is very lightly dependent on photons energy. In our case the optimal diameter for cylindrical indium sample is about 6.4 cm. This value is always related to the particular detector dimensions as it was said in point 2.

During of the activation process, the mass of the sample plays an important role because the number of activated nuclei in the target sample is strictly dependent on the sample mass. The Integrated Mass Absolute Full Energy Peak Efficiency IMAFEPE is a definite Riemann integral of mass and efficiency product and takes into account both the reactivity of the sample and the efficiency of the HPGe detector.

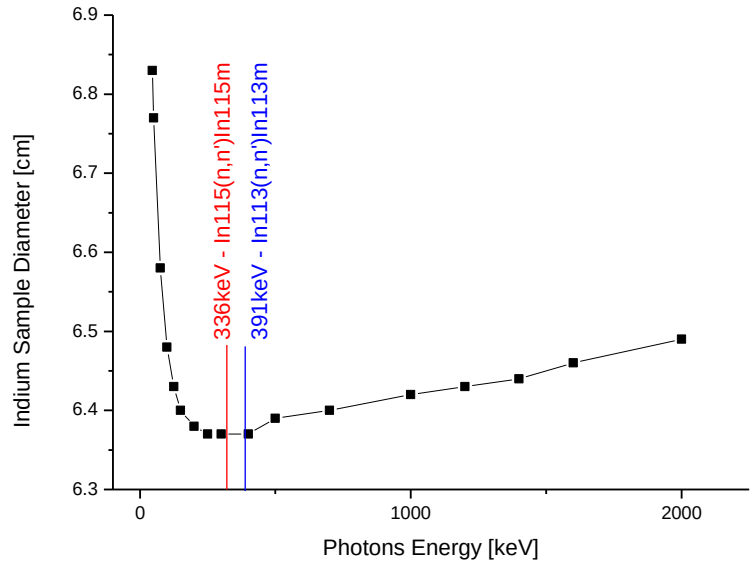

Fig. 5. Inflection points represent the interval of optimal diameters

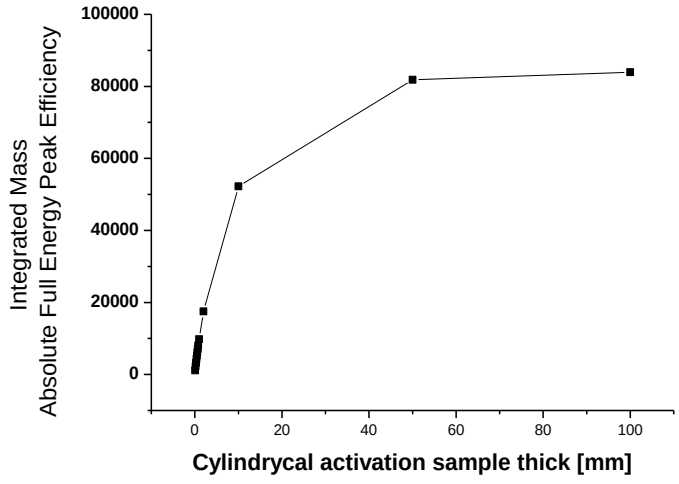

Fig. 6. The Integrated Mass Absolute Full Energy Efficiency represents the ability of particular sample geometry simultaneously for activation and further its measurability by the gamma spectrometry

Fig. 6 demonstrates that increasing the sample thickness can in principle lead to the infinite increase of IMAFEPE. This process is very rapid for the first few centimeters of sample thickness but then the self shielding effect starts reducing the number of photon escaping from sample and reaching the detector. It could be also noted that there is no one strictly defined optimal thickness for cylindrical samples.

Based on these results it was noted that realistic indium samples should have an chosen diameter to fulfill all the optimization requirements mentioned above. This plays a particularly important role when the number of neutrons activating the sample is very limited.

Absolute Full Energy Peak Efficiency for stack of different foils and for samples made of mixture of elements activated during recent JET campaigns

A set of metal foils with 18mm diameter but with different thicknesses have been used during recent JET campaigns. The process of sample efficiency calibration with calibration sources is usually expensive, very complex to carry out and its accuracy is very limited. This method would limit the number of samples which could be used during the activation experiments. The numerical characterization of HPGe detector gives practically unlimited access to a wide number of activation materials with different geometry and density. In Fig. 7A-D essential data is presented for eleven different metal foils (with this same sample geometry - diameter and thickness and measurement geometry) used on JET during the C20-C26 campaigns. The eleven metals used are: aluminium, indium, yttrium, titanium, zirconium, iron, cadmium, nickel, cobalt, hafnium and gold. The lighter sample has been made of aluminum and weights 0,7 g whereas the heavier sample has been made of gold and weighs 4,9 g. Fig. 7A presents the Absolute Full Energy Peak Efficiency for all these samples. Each metal has a different density and this influences the sample mass (Fig. 7D), the maximum value of efficiency-AFEPE (Fig. 7B), the energy position of the maximum efficiency peak (Fig. 7F), the size of the field under the efficiency curve-IAFEPE (Fig 7C) and the mass-efficiency factor –MIAFEPE (Fig. 7E). Increasing the atomic number of the used element results in decreasing IAFPE and maximum value of AFEPE and in an increase of the photon energy corresponding to the peak of maximum AFEPE and MIAFEPE.

In the previous experiments on JET only stacks of different discrete foils were usually used. One of the main disadvantages of such an activation method is the high number of measurements to be performed after a single activation experiment since only one sample can be analyzed at any given time by a single detector.

The numerical characterization of the detector allows estimation the efficiency calibration both for the mixture of nuclides and for different sample geometries. On the base of this approach a novel kind of sample consisting of multi-elements mixture (“mixed sample”) were designed, prepared and used at JET. They have been manufactured by pressing the powders of Al, Se, Y, Au, Fe element. This technique allows measurement of a higher number of nuclear reaction occurring in one activation then previously. It also allows measurement of short-lived nuclides because they all are measured at the same time [7]. Fig 8 presents three different efficiency curves for activation samples including the efficiency curve for mixed activation samples. The above mentioned mixture has a relatively high efficiency of photon registration and allows measuring significantly more nuclear reactions during one measurement scan.

Conclusions

The performed analysis proves the applicability of the proposed mixed sample technique to characterize the neutron yield in large fusion devices like JET and ITER [8].

In the case of activation of samples made from different metals, the higher density sample has the smaller AFEPE because of increased self shielding effect.

Optimization of the sample size allows effective use of the activation technique in irradiation positions with relatively low neutron fluence.

It has been shown that there is no strong dependence between the value of the optimal sample diameter and the photon energy. The optimal diameter for the real sample is a crucial parameter which has unique value for any particular HPGe detector.

It has been also shown that the accuracy of efficiency calibration performed by Labsocs in comparison with the efficiency calibration done with standard source solutions is very accurate if sample geometry, composition, and density are well defined.

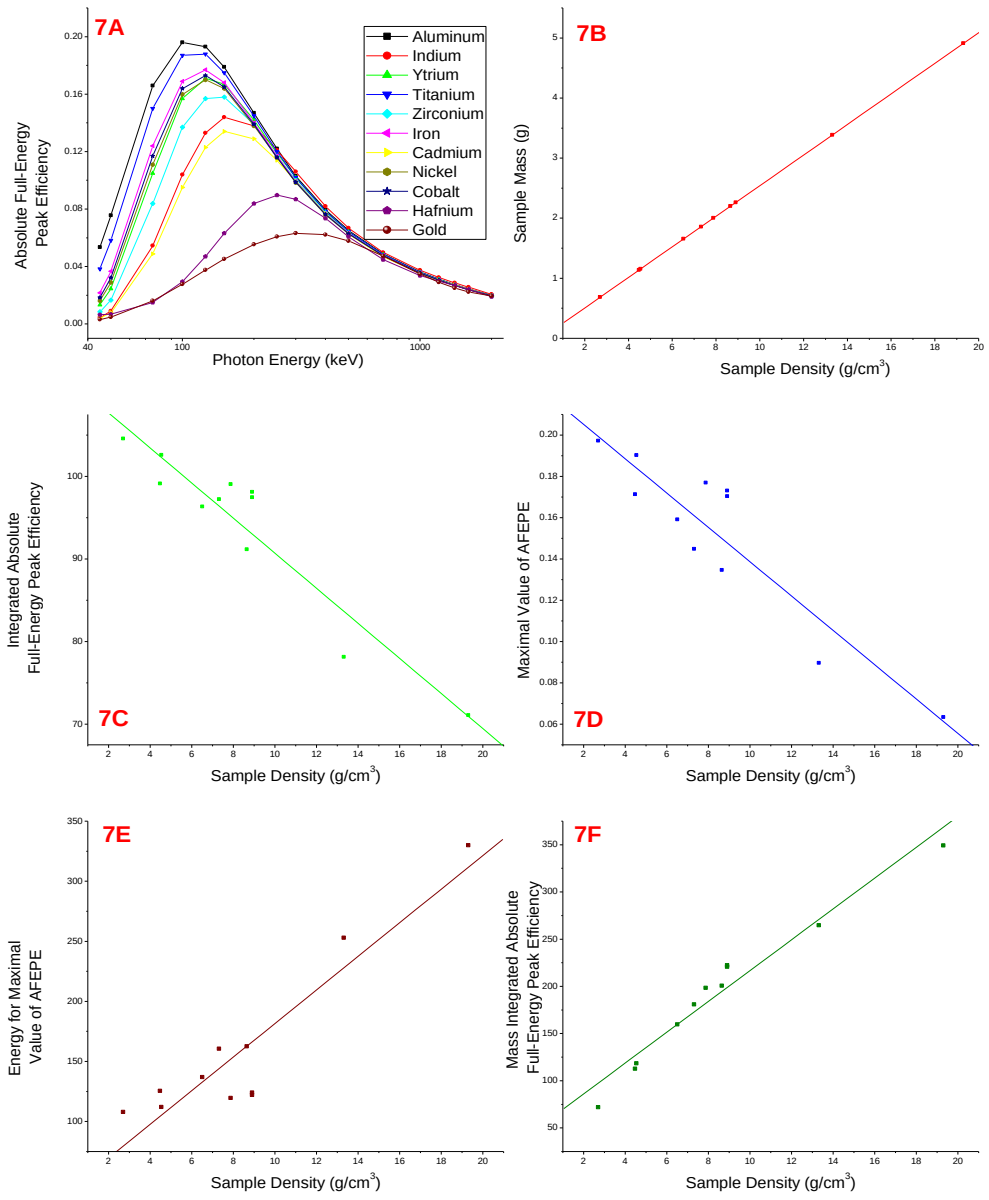

Fig. 7. Fig. 7A shows AFEPE for different activation samples with identical geometry: diameter 18 mm and thickness 1 mm. Fig. 7B presents how sample mass depends on density. Fig. 7C presents increasing of MIAFEPE as a factor depending of sample density. MIAFEPE it is a product of sample mass of sample (Fig 7D) and IAFEPE (Fig. 7E). The increasing of sample density which is a function of atomic mass influents on transfer a peak of maximum efficiency to higher energy area (Fig. 7E). Dependence of maximum value of efficiency for particular sample on sample density which simultaneously manifests the general process of decreasing of efficiency with the increasing of atomic number of element which has been used for sample fabrication

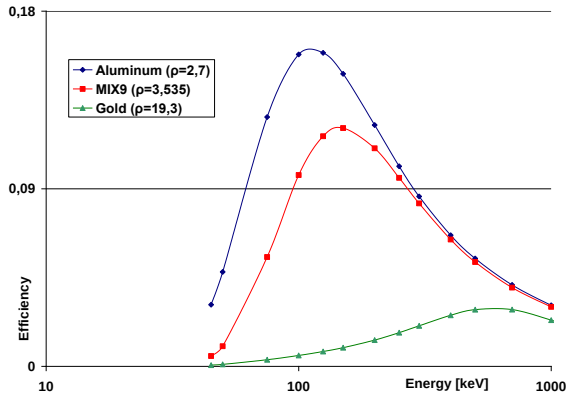

Fig. 8. AFEPE for realistic sample with 18mm diameter and 5,6mm thick made of three different materials. The efficiency of mixed sample (named MIX9) is relatively high nevertheless it consists of Al, Se, Y, Au, Fe. It is insignificantly lower from light aluminum and higher than in heavy gold case

References

[1] B. Esposito, L. Bertalot, M. Louglin, A. L. Roquemore, Neutron spectrum measurements in DT discharges using activation technique, Rev. of Sci. Instrum. (1999) **70** (1), 1130-1133.
[2] L. Bertalot, L. Roquemore, M. Louglin, B. Esposito, Calibration of the JET neutron activation system for DT operation, Rev. of Sci. Instrum (1999) **70** (1), 1137-1140.
[3] R.Prokopowicz, B.Bieńkowska, K.Drozdowicz, S.Jednoróg, E.Kowalska-Strzęciwilk, A.Murari, S.Popovichev, K.Pytel, M.Scholz, A.Szydłowski, B.Syme, G.Tracz, and JET-EFDA contributors*, Measurements of neutrons at JET by means of the activation methods, in printing.
[4] Practical gamma-ray spectrometry, G. Klimor, J. D. Hemingway, pp 137-138, Chichestrer, New York, Brisbane, Toronto, Singapore, 1995.
[5] F.L. Bronson, R. Venkataraman, Validation of the accuracy of the LabSOCS mathematical Efficiency calibration for typical laboratory samples, 46th Annual Conference on Bioassay, Analytical and Environmental Radiochemistry, November 12-17, 2000, Seattle, Washington DC.
[6] F.L. Bronson; R. Venkataraman, B. Young, Massemetric efficiency calibrations of Ge detectors for Laboratory applications, 44th Annual Conference on Bioassay, Analytical and Environmental Radiochemistry, November 15-19, 1998; Albuquerque NM.
[7] M. Scholz, S. Jednoróg, A. Murari, S. Popovichev, R. Prokopowicz, A.Szydłowski and JET EFDA contributors Neutron Measurements near JET Vacuum Vessel Surface by Multi-Elements Activation Method, Proceedings of the 36th EPS Conference on Plasma Physics, Sofia, Bulgaria, 2009.
[8] C. Barnes, M. Louglin, T. Nishitani, Neutron activation for ITER, Rev. of Sci. Instrum. (1997) **68** (1), 577-580.
[9] F. Romanelli et al, "Overview of JET Results", Proc. 22nd IAEA Fusion Energy Conference, Geneva, Switzerland, 2008.